

A Sliding-Mode-Like Position Controller for Admittance Control with Bounded Actuator Force

Ryo Kikuuwe, *Member, IEEE*

Abstract—This paper proposes a new position controller that is suitable for the use as the internal position servo of an admittance controller with bounded actuator forces. The new position controller approximately behaves as a proportional-integral-derivative (PID) controller with an acceleration feedforward in normal situations and as a sliding mode controller when the actuator force is saturated. The admittance controller employing the new position controller realizes smooth transitions between saturated periods and unsaturated periods. Moreover, it quickly responds to changes in the applied force even when the actuator force is saturated, leading to better stability and smoothness. The controller was validated through experiments using a robotic manipulator.

Index Terms—Position control, admittance control, force control, sliding mode

I. INTRODUCTION

When a robotic manipulator is working in contact with external environment, an appropriate controller is necessary to control the contact force between the robot's end-effector and the environment. Many control strategies have been proposed so far as overviewed in some previous survey papers [1], [2]. In situations where a force sensor is available in the end-effector and the robot's joints have high friction, a reasonable choice is the class of control methods that are generally termed as admittance control [3]–[5].

A typical implementation of admittance control is illustrated in Fig. 1. In this type of controllers, a virtual object having simple dynamics is considered in the controller, the force-sensor signal is used to simulate the object's motion according to the force, and the robot is position-controlled so as to track the resultant object's motion. As long as the internal position control is accurate enough, the robot's response to external forces is close to that of the virtual object. This control framework has been applied to haptic rendering [4], [5], teleoperation [6], rehabilitation [7], [8], human-machine collaboration [9], and some manufacturing processes [10].

In most applications, the magnitudes of robots' actuator forces¹ are limited due to hardware limitations or safety reasons. The actuator force can saturate especially when there is an abrupt change in the virtual object's velocity and when a large external force is applied to the robot. One problem of the actuator force saturation in admittance control is that, when the actuator force saturates, the robot's position can be

The author is with Department of Mechanical Engineering, Kyushu University, 744 Motooka, Nishi-ku, Fukuoka 819-0395, Japan. The corresponding author is Ryo Kikuuwe (e-mail: kikuuwe@ieee.org, phone: +81-92-802-3174, fax: +81-92-802-0001).

¹This paper uses the term "force" to mean a generalized force, which is a torque in rotational systems.

far separated from the virtual object's position, resulting in undesirable behaviors such as oscillation, repeated overshoots, and instability. System behaviors in such a situation are not studied in detail in the literature. Increasing damping and inertia of the virtual object contributes to preventing the saturation, but it results in poor responsiveness against the contact force and thus is not suitable for many applications.

This paper proposes a new position control law that can be used as an internal position controller of an admittance controller for achieving better post-saturation behavior. It is an extension of a Proxy-based Sliding Mode Control (PSMC) proposed by the author and his colleagues [11], which is a discrete-time approximation of a simple sliding mode controller and also is an extension of a saturated PID controller. In contrast to PSMC, the new controller employs a higher-dimensional sliding surface in the state space spanned by position, velocity, and acceleration, and includes a feedforward term of the desired acceleration. When the actuator force saturates, the controller approximately behaves as a sliding mode controller with the higher-dimensional sliding surface, which enables smooth transitions between saturated and unsaturated periods and quick response against the measured force. Meanwhile, when the actuator force is not saturated, it behaves as a PID controller with acceleration feedforward, which realizes better stability than the plain PID controller without feedforward.

The remainder of the paper is organized as follows. Section II overviews previous works on admittance control. Section III provides a preliminary theoretical discussion on admittance control and sliding mode position control with the higher-dimensional sliding surface. Section IV presents the new position controller. Section V shows experimental results, and Section VI provides concluding remarks.

II. RELATED WORK

Early versions of admittance control, which employs an internal position loop and an external force loop, can be found

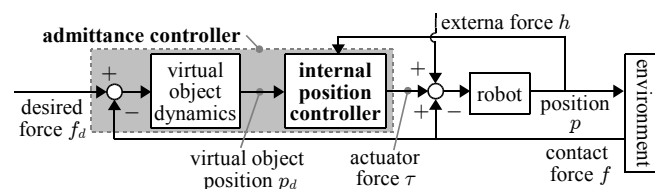


Fig. 1. Block diagram of an admittance-controlled robot in contact with an environment.

in the literature since the 1970s. Those controllers can be classified into explicit force controllers [12]–[14] and impedance controllers [15]–[18]. The former is to control the force on the end-effector and the latter is to control the apparent mechanical impedance of the end-effector. Those two types can be realized in similar frameworks to each other, between which the only difference is whether a desired force command is provided or not. Those controllers have been referred to by various names, such as “virtual internal model following control” [10], [19], “position-based impedance control” [20], [21], and “admittance control” [4], [5], [7], [9].

Stability has been a primary concern of admittance controllers. Main sources of instability are time delay in the controller [13], [22] and the limited bandwidth [23]–[25] of the internal position-controlled subsystem. It has been known that the virtual mass and viscosity should be set high to suppress the instability. It has also been suggested to set the virtual mass to be equal to the real mass of the device to suppress the influence of joint friction [26], [27]. A large virtual mass or viscosity, however, is not desirable for some applications because it can deteriorate the responsiveness of the controller. As another type of approach to enhance the stability, some of previous studies employ internal position controllers with feedforward terms to compensate the effect of the robot's dynamics [4], [28]–[30], which can be viewed as phase-lead compensators.

The actuator saturation has not been studied in depth in the literature, except in the context of how it should be avoided. As far as the author is aware, the only analytical study in this regard is González and Widmann's one [31]. They pointed out that the saturation increases the stability bound in terms of the sampling interval because it temporarily makes the system equivalent to an open-loop system. They however do not consider the situation where positive and negative saturation repeatedly occur one after the other, which is usually undesirable.

There are some force control schemes that do not involve internal position loops. One of major approaches is to employ proportional-integral (PI) feedback of the force error [32], [33] and some sophisticated terms considering the dynamics of the robot [34]. One disadvantage of such an approach is that it results in the robot's interactive behavior being strongly dependent on the dynamics of the environment and the robot. In particular, the joint Coulomb friction is one of the biggest sources of performance deterioration, as has been discussed in [35]. Acceleration-based methods [36]–[38] may achieve better contact stability, but they require pre-identified model of joint friction when the friction is not negligible [38]. Force controllers of these classes will not be considered any further in this paper.

III. PRELIMINARY ANALYSIS

A. Mathematical Preliminaries

For the discussion in the upcoming sections, let us define the following two functions:

$$\text{sgn}(x) \triangleq \begin{cases} x/|x| & \text{if } x \neq 0 \\ [-1, 1] & \text{if } x = 0 \end{cases} \quad (1)$$

$$\text{sat}(x) \triangleq x / \max(1, |x|). \quad (2)$$

They are related by the following theorem:

Theorem 1. *With any pairs of real numbers x and y ,*

$$y = \text{sgn}(x - y) \iff y = \text{sat}(x) \quad (3)$$

is satisfied.

Proof: It can be proven as follows:

$$\begin{aligned} y = \text{sgn}(x - y) &\iff ((y \in [-1, 1]) \wedge (x - y = 0)) \vee \\ &((y = 1) \wedge (x - y > 0)) \vee ((y = -1) \wedge (x - y < 0)) \\ &\iff ((y = x) \wedge (x \in [-1, 1])) \vee ((y = 1) \wedge (x > 1)) \\ &\vee ((y = -1) \wedge (x < -1)) \iff y = \text{sat}(x). \quad \blacksquare \end{aligned}$$

As a direct consequence of Theorem 1, one can see that, for any positive scalars X, Y, Z and scalars x, y, z , the following relation is satisfied:

$$\begin{aligned} Xy - z &= Y\text{sgn}(x - Zy) \\ &\iff Xy - z = Y\text{sat}((Xx/Z - z)/Y). \quad (4) \end{aligned}$$

In Section IV, the new controller will be presented in a continuous-time representation involving the discontinuous sgn function, but, by using Theorem 1 or the relation (4), it will be converted into a discrete-time algorithm involving the continuous sat function.

B. 1-DOF System

In order to motivate the new controller, this section addresses a one-dimensional robot consisting of a point mass subject to admittance control in contact with an environment. Fig. 1 illustrates a block diagram of this system.

Let $p \in \mathbb{R}$ and $M_r > 0$ be the position and the mass of the robot, respectively. Let $f \in \mathbb{R}$ be the force acting from the robot to the environment, τ be the actuator torque acting on the robot, and h be the force acting on the robot from all other sources. Then, the equation of motion of the robot can be written as follows:

$$M_r \ddot{p} = \tau - f + h. \quad (5)$$

An admittance controller with a desired force input $f_d \in \mathbb{R}$ can be constructed as a combination of a simulator of a virtual object's motion and a position controller for forcing the robot to follow the virtual object's motion. One example of such a controller can be described as follows:

$$\ddot{p}_d = (-b\dot{p}_d - f + f_d)/m \quad (6)$$

$$\tau = M\ddot{p}_d + B(\dot{p}_d - \dot{p}) + K(p_d - p) + L \int (p_d - p) dt. \quad (7)$$

Here, m, b, K, B, L and M are positive constants. The inputs are the force f and the position p measured by sensors and the desired force f_d . The output is the actuator force τ . Equation (6) describes the dynamics of the virtual object (of which the mass is $m > 0$, the viscosity is $b > 0$, and the position is $p_d \in \mathbb{R}$) subject to an external force f and the input force f_d . Equation (6) can also be interpreted as a controller to make the measured force f track the desired value f_d .

Equation (7) is the internal position controller, which accepts the desired position input p_d . In this controller, K, B

and L are P-, D- and I-gains, respectively. The term $M\ddot{p}_d$ is for compensating the inertial term $M_r\ddot{p}$ of the robot dynamics (5). Such a term has been employed by some researchers [4], [19], [39], and its effects have been experimentally tested in [4]. The role of this feedforward term can be understood as a phase-lead compensator that reduces the phase lag from p_d to p . This term improves the stability of the system in the presence of the feedback loop from p to f , which is generated when the robot is in contact with an environment.

The stability of the admittance-controlled system in contact with an environment can be analyzed based on transfer functions, if the environment response is linear. However, there is always a magnitude limit on the actuator force τ , and thus the force τ can easily saturate especially when K is large. In this case, the controller can be viewed as a nonlinear controller, which is difficult to analyze through the linear control theory.

C. PD-type Sliding Mode Position Controller

One of major problematic situation involving actuator saturation is repeated transitions between negative saturation and positive saturation. The possibility of occurrence of such a situation is now investigated. Instead of (7), let us consider a very-high-gain PD controller with an actuator saturation, which can be approximated as follows:

$$\tau = F \text{sgn}(s) \quad (8)$$

where

$$s \triangleq p_d - p + H(\dot{p}_d - \dot{p}). \quad (9)$$

This controller (8) is equivalent to the following:

$$\tau = \lim_{\kappa \rightarrow \infty} F \text{sat}(\kappa s / F), \quad (10)$$

which implies that (8) can be considered as a PD controller with extremely high gains. It would be possible to refer to (8) as a PD-type sliding mode controller.

In order to analyze the behavior of the controller (8), let us substitute (8) into (5). Then, considering the first-order derivative of s , one can obtain the following equation of motion:

$$M_r\ddot{p} + f - h = \lim_{\varepsilon \rightarrow 0} F \text{sgn}(s + \varepsilon \dot{s}). \quad (11)$$

Here, note that $\dot{s} = \dot{p}_d - \dot{p} + H(\ddot{p}_d - \ddot{p})$ and that \ddot{p} is contained both in the right- and left-hand sides of (11). By using (4), one can remove \ddot{p} in the right-hand side, obtaining the following:

$$\ddot{p} = \begin{cases} (F \text{sgn}(s) - (f - h)) / M_r & \text{if } s \neq 0 \\ \frac{F}{M_r} \text{sat}\left(\frac{M_r}{F}\left(\ddot{p}_d + \frac{\dot{p}_d - \dot{p}}{H}\right) + \frac{f - h}{F}\right) - \frac{f - h}{M_r} & \text{if } s = 0. \end{cases} \quad (12)$$

Furthermore, by substituting (12) into (5), one can see that τ satisfies the following:

$$\tau = \begin{cases} F \text{sgn}(s) & \text{if } s \neq 0 \\ F \text{sat}\left(\frac{M_r}{F}\left(\ddot{p}_d + \frac{\dot{p}_d - \dot{p}}{H}\right) + \frac{f - h}{F}\right) & \text{if } s = 0. \end{cases} \quad (13)$$

This means that a transition from the sliding mode ($s = 0$) to the reaching mode ($s \neq 0$)² occurs when the condition

$$\dot{p} \in (\dot{p}_d + H\ddot{p}_d + (H/M_r)(f - h - F[-1, 1])) \quad (14)$$

is violated.³

A transition of the opposite direction, i.e., from the reaching mode to the sliding mode, happens when the state $\{p, \dot{p}\}$ crosses the line $s = 0$ in the state space. In order that the state remains in the sliding mode, the condition (14) must be fulfilled, and otherwise repeated transitions occur between negative saturation and positive saturation. Equation (14) shows that the condition can be violated when the speed $|\dot{p}|$ is high, although an increase of H enlarges the range of \dot{p} for the state being captured in the sliding mode.

Another point that should be noticed is that, as can be seen from (13), the actuator force τ changes discontinuously at a transition from the reaching mode to the sliding mode. Although it is the case only when κ (in (10)) is infinite, a large κ results in abrupt changes in τ . When such a discontinuous change occurs, the admittance-controlled robot behaves as if f or f_d discontinuously changes. This is clearly an undesirable effect especially when the robot is supposed to physically interact with human users.

D. PDD²-type Sliding Mode Position Controller

To overcome the problems of the repeated saturation and the actuator force discontinuity, let us consider the following internal position controller:

$$\tau = F \text{sgn}(\sigma) \quad (15)$$

where

$$\sigma \triangleq p_d - p + H(\dot{p}_d - \dot{p}) + J(\ddot{p}_d - \ddot{p}). \quad (16)$$

This controller can be viewed as an extreme case of a PDD² (proportional, derivative, and second derivative) controller with extremely high gains because (15) is equivalent to the following:

$$\tau = \lim_{\kappa \rightarrow \infty} F \text{sat}(\kappa \sigma / F). \quad (17)$$

It would be possible to refer to (15) as a PDD²-type sliding mode controller.

Under this control law, the equation of motion of the position-controlled subsystem can be described as follows:

$$M_r\ddot{p} + f - h = F \text{sgn}(\sigma). \quad (18)$$

By using (4), (18) can be rewritten as follows:

$$\ddot{p} = \frac{F}{M_r} \text{sat}\left(\frac{M_r}{F}\left(\ddot{p}_d + \frac{\dot{p}_d - \dot{p}}{J}\right) + \frac{f - h}{F}\right) - \frac{f - h}{M_r}. \quad (19)$$

Moreover, by substituting (5) by (19), one can see that the following is satisfied:

$$\tau = F \text{sat}\left(\left(\frac{M_r}{F}\right)\left(\ddot{p}_d + \frac{\dot{p}_d - \dot{p}}{J}\right) + \frac{f - h}{F}\right). \quad (20)$$

²It must be noted that the actuator force is saturated in the reaching mode ($s \neq 0$) and is not saturated in the sliding mode ($s = 0$).

³This paper adopts the notation in which, for any scalars x , y , and z , $x + [y, z]$ means $[x + y, x + z]$. This notation is consistent with the one that has often been used in the field of differential inclusion, e.g., [40].

Equation (20) implies that the state is in the sliding mode ($\sigma = 0$) as long as

$$(p + H\dot{p}) \in \left(p_d + H\dot{p}_d + J\ddot{p}_d + \frac{J(f-h)}{M_r} - \frac{FJ}{M_r}[-1, 1] \right) \quad (21)$$

is satisfied. This means that the sliding mode can be achieved even when the velocity \dot{p} is high, while it is not the case with the PD type (8). Equation (20) also shows that the actuator torque τ is always continuous unless there is a discontinuity in \ddot{p}_d , f , or h . Under admittance control, a discontinuity in \ddot{p}_d is only resulted from discontinuities in the external force f or the commanded force f_d . This means that the discontinuities in \ddot{p}_d , f , or h are properly reflected in τ .

Equation (19) shows that, in the sliding mode, p converges to p_d along a smooth trajectory characterized by H and J , without being disturbed by f and h . If $J \leq H^2/4$, the converging trajectory is overdamped and thus no overshoots are produced.

One must note that the controller (15) cannot be realized in practice because it involves a high-gain acceleration feedback without latency. It is however possible to derive some theoretical properties of (15) applied to the one-dimensional robot (5). The following two propositions are relevant to the upcoming discussion:

Proposition 1 (Stability of a rigid mass under the position controller (15)). *Consider the system described by (5) and (15), and assume that $f = h = 0$ and $\dot{p}_d = 0$. Then, the system is globally asymptotically stable at the equilibrium $\dot{p} = 0$ and $p = p_d$.*

Proposition 2 (Stability of a rigid mass in contact with an elastic environment under the admittance controller (6)(15)). *Consider the system described by (5), (6), and (15), and assume that f_d is a constant satisfying $|f_d| < F$, $h = 0$, and $f = K_e p$. Here $K_e > 0$ is a constant. Then, the system is locally asymptotically stable at the equilibrium $\dot{p} = \dot{p}_d = 0$ and $p = p_d = f_d/K_e$.*

The proofs are provided in Appendix. It should be noted that, at this time, the globality of Proposition 2 has not been proven.

E. Differential-Algebraic Implementation

As has been pointed out in the previous section, the aforementioned two discontinuous position controllers, (8) and (15), cannot be realized in practice because of the inevitable latency in the controller. One imaginable remedy is to smooth the discontinuities of (8) and (15), respectively, as follows:

$$\tau = F \text{sat}(Ks/F) \quad (22)$$

$$\tau = F \text{sat}(K\sigma/F) \quad (23)$$

where K is a positive constant of a finite value. This approach has been known as a ‘‘boundary layer’’ [41], [42] approach, where the discontinuity of sgn is smoothed in the boundary layer $|s| < F/K$ or $|\sigma| < F/K$. This approach, however, does not always provide usable control laws. As for the controller (22), it employs the derivative feedback of the gain KH , which can be so high that the noise in the velocity measurement can

be excessively magnified. The controller (23) requires a high-gain acceleration feedback, which is also difficult in practice.

The previous paper [11] proposed a Proxy-based Sliding Mode Control (PSMC), which is an alternative approximation of the PD-type sliding mode controller (8). The continuous-time representation of PSMC can be described as the following differential-algebraic equation:

$$\tau = B\ddot{a} + K\dot{a} + La \quad (24a)$$

$$\tau = F \text{sgn}(s - \dot{a} - H\ddot{a}). \quad (24b)$$

Here, $a \in \mathbb{R}$ is a state variable newly introduced, and K , B , and L are appropriate positive constants. The expression (24) can be viewed as a set of simultaneous differential equations with respect to τ and a , and (24) becomes close to the PD-type sliding mode controller (8) as K increases. Although (24) involves the discontinuous function sgn , it is in fact a continuous controller. This can be seen through the fact that, by using the relation (4), (24) can be equivalently rewritten as follows:

$$\ddot{a} = -\frac{K\dot{a} + La}{B} + \frac{F}{B} \text{sat} \left(\frac{B}{F} \left(\frac{s - \dot{a}}{H} + \frac{K\dot{a} + La}{B} \right) \right) \quad (25a)$$

$$\tau = F \text{sat} \left(\frac{B}{F} \left(\frac{s - \dot{a}}{H} + \frac{K\dot{a} + La}{B} \right) \right), \quad (25b)$$

which involves only continuous functions.

One possible physical interpretation of the controller (24), or equivalently (25), is illustrated in Fig. 2. Here, $p_s \triangleq p + \dot{a}$ can be interpreted as the position of a ‘‘proxy,’’ which is a virtual massless object. The term ‘‘proxy’’ is borrowed from the area of haptic rendering (e.g., [43]), and, in this paper, it has nothing to do with the virtual object in an admittance controller. The proxy is connected to the real controlled object through a PID controller (24a), and is also connected to the desired position p_d (which is the position of the virtual object used in admittance control) through a sliding mode controller (24b). Because the proxy has no mass, the forces generated by the two controllers balance with each other, and thus τ is used in both (24a) and (24b). Equation (24b) implies that $p_d - p_s + H(\dot{p}_d - \dot{p}_s) = 0$ is satisfied in the unsaturated period and the robot position p is controlled to follow the proxy position p_s as the effect of the PID controller (24a). It is easy to see that, as K increases, p_s approaches p . This means that the controller (24) approximates the PD-type sliding mode controller (8) that does not involve a high-gain velocity feedback.

The controller (8) also has some limitations as the internal position controller of an admittance controller. One is that,

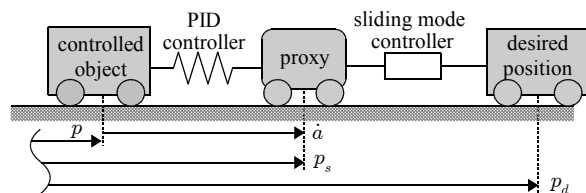


Fig. 2. A physical interpretation of the controller (24). The desired position p_d is the input to the controller and also is the virtual object position in the case of admittance control.

because (8) is close to (13) when K is high, it also produces discontinuous actuator force at a transition from the reaching mode to the sliding mode. In addition, in the sliding mode, (8) is equivalent to a *plain* PID controller, which does not have the term $M\ddot{p}_d$ in (7) for improving the contact stability.

IV. NEW CONTROLLER

A. New Position Controller

The previous section has shown that PDD²-type sliding mode controller (15) has some theoretical advantages but cannot be implemented through the conventional boundary layer approach. Now, let us consider realizing the PDD²-type sliding mode control with a differential-algebraic approximation, which is described as follows:

$$\tau = M\ddot{p}_d + B\ddot{a} + K\ddot{a} + La \quad (26a)$$

$$\tau = F\text{sgn}(\sigma - (\dot{a} + H\ddot{a} + J\ddot{\ddot{a}})). \quad (26b)$$

Here, a is an internal state variable memorized in the controller and K, B, L, H, J, M and F are non-negative constants. The controller (26) accepts the inputs of the current position p and the desired position p_d , makes the state a evolve, and provides the output of the actuator torque τ .

By substituting $M = 0$ and $J = 0$, the controller (26) reduces to (24), which is PSMC in the authors' previous paper [11]. In the controller (26), the term $M\ddot{p}_d$ is to expand the bandwidth of the position-controlled system by compensating the effect of the robot inertia M_r , as discussed in section III-B. This term enhances the contact stability in the sliding mode. The term $J(\ddot{p}_d - \ddot{p} - \ddot{\ddot{a}})$ in (26b) is to approximately realize the PDD²-type sliding mode discussed in section III-D.

A physical interpretation of (26) can also be explained by using Fig. 2. The proxy position corresponds to $p_s \triangleq p + \dot{a}$, as was also the case with PSMC. The PID controller is replaced by (26b), which has the additional acceleration feedforward term, and the sliding mode controller is replaced by (26a), which is now of the PDD² type. It is easy to see that, as K increases, p_s approaches p and the controller (26) becomes close to the PDD²-type sliding mode controller (15).

B. Discrete-Time Implementation

Here, we derive a discrete-time algorithm of the controller (26). By using the backward Euler scheme, a discrete-time approximation of (26) can be obtained as follows:

$$\tau(k) = F\text{sgn}(\tau^*(k) - \tau(k)) \quad (27a)$$

$$\tau(k) = \tau_f(k) + (Ba(k-2) - (2B+K)a(k-1) + (B+KT+LT^2)a(k))/T^2 \quad (27b)$$

where

$$\tau^*(k) \triangleq \tau_f(k) + C_s\sigma(k) + C_1a(k-1) - C_2a(k-2) + C_3a(k-3) \quad (28)$$

$$\tau_f(k) \triangleq M\nabla^2 p_d(k)/T^2 \quad (29)$$

$$\sigma(k) \triangleq p_d(k) - p(k) + H\nabla(p_d(k) - p(k))/T + J\nabla^2(p_d(k) - p(k))/T^2 \quad (30)$$

and

$$C_s \triangleq \frac{T(B+KT+LT^2)}{J+HT+T^2} \quad (31)$$

$$C_1 \triangleq \frac{KH-B+LT(2H+T)}{J+HT+T^2} + \frac{J(B+2KT+3LT^2)}{T^2(J+HT+T^2)} \quad (32)$$

$$C_2 \triangleq \frac{(K+LT)H-B}{J+HT+T^2} + \frac{J(2B+3KT+3LT^2)}{T^2(J+HT+T^2)} \quad (33)$$

$$C_3 \triangleq \frac{J(B+KT+LT^2)}{T^2(J+HT+T^2)}. \quad (34)$$

Here, k is an integer that denotes a discrete-time index, $T > 0$ is the time-step size, and ∇ denotes the backward difference operator, which is defined as $\nabla x(k) = x(k) - x(k-1)$ and satisfies $\nabla^2 x(k) = x(k) - 2x(k-1) + x(k-2)$.

Equation (27) is a set of simultaneous equations with the unknowns $\tau(k)$ and $a(k)$. By using Theorem 1, (27a) can be rewritten as follows:

$$\tau(k) = F\text{sat}(\tau^*(k)/F). \quad (35)$$

By noticing that $\tau^*(k)$ is independent from the unknowns $\tau(k)$ and $a(k)$, one can see that (35) is the closed-form solution for $\tau(k)$. The other unknown $a(k)$ can be obtained through (27b).

In conclusion, the differential-algebraic equation (26) can be numerically solved with the following computational procedure:

$$\tau_f(k) := M\nabla^2 p_d(k)/T^2 \quad (36a)$$

$$\sigma(k) := p_d(k) - p(k) + H\nabla(p_d(k) - p(k))/T + J\nabla^2(p_d(k) - p(k))/T^2 \quad (36b)$$

$$\tau^*(k) := \tau_f(k) + C_s\sigma(k) + C_1a(k-1) - C_2a(k-2) + C_3a(k-3) \quad (36c)$$

$$\tau(k) := F\text{sat}(\tau^*(k)/F) \quad (36d)$$

$$a(k) := ((2B+KT)a(k-1) - Ba(k-2) + T^2(\tau(k) - \tau_f(k)))/(B+KT+LT^2). \quad (36e)$$

This is the controller algorithm to provide the actuator force $\tau(k)$ according to the measured position $p(k)$ and the desired position $p_d(k)$. By setting $M = 0$ and $J = 0$, (36) reduces to the algorithm of PSMC, which is Equation (32) of [11].

C. Properties of New Position Controller

The properties of the new position controller (36) are now discussed based on its continuous-time representation (26). For the convenience of discussion, let us define $c \triangleq Ka$, $\hat{B} \triangleq B/K$, $\hat{L} \triangleq L/K$. Then, (26) can be rewritten as follows:

$$\tau = F\text{sgn}(\sigma - (\dot{c} + H\ddot{c} + J\ddot{\ddot{c}})/K) \quad (37a)$$

$$\tau = M\ddot{p}_d + K(\hat{B}\ddot{c} + \dot{c} + \hat{L}c). \quad (37b)$$

As K goes to the infinity, the system (37) is decoupled into the following two subsystems:

$$\tau = F\text{sgn}(\sigma) \quad (38a)$$

$$\ddot{c} = -(\dot{c} + \hat{L}c)/\hat{B}. \quad (38b)$$

This means that the controller (26), or equivalently (37), is an approximation of the PDD²-type sliding mode controller (15).

By careful observation on (26), it can be seen that $p_s = p + \dot{a}$ evolves so that $p_d - p_s + H(\dot{p}_d - \dot{p}_s) + J(\ddot{p}_d - \ddot{p}_s) = 0$ is maintained as long as this p_s value results in τ that does satisfy $|\tau| < F$. During this period, (26) behaves as a PID controller with acceleration feedforward. If the resultant τ does not satisfy $|\tau| < F$, p_s evolves so that

$$\pm F = M\ddot{p}_d + B(\dot{p}_s - \dot{p}) + K(p_s - p) + L \int (p_s - p) dt \quad (39)$$

is satisfied. This means that the actual acceleration \ddot{p} is not used in the controller and that the velocity feedback is performed only with the gain B , which does not have to be so high as to produce overdamped response. In this sense, the differential-algebraic approximation (26) is inherently different from the simple boundary layer approximation (23).

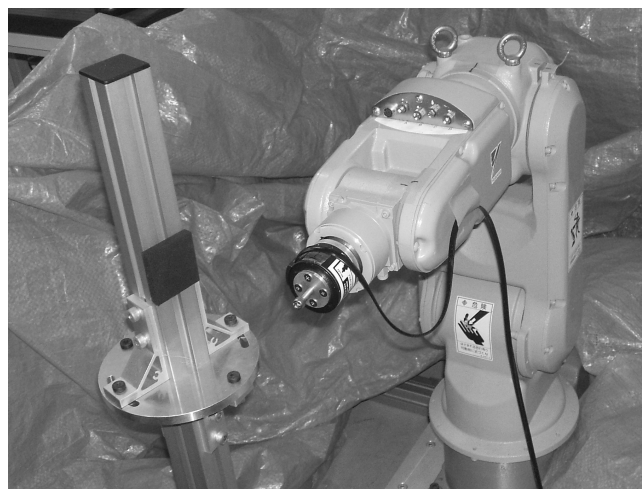
Strict stability analysis on the new controller (26) is still an open problem. The special case of (26) with $J = 0$ and $M = 0$ has been analyzed in [11], but the term $J\ddot{a}$ prevents the application of the same approach to the case of $J > 0$. A possible approach is to employ (15) as an approximation of (26). As long as the PID controller (26a) in (26) is stable and K is high enough, the proxy position $p_s = p + \dot{a}$ is close to the actual position p , and thus Propositions 1 and 2 in section III-D is approximately applicable to the controller (26). Under the condition that the PID controller (26a) is accurate enough (by appropriate choice of $\{M, K, B, L\}$), Proposition 1 suggests that the position controller (26) is stable with a constant p_d and $h = f = 0$. Under the same condition, Proposition 2 suggests that an admittance controller comprising (26) is locally asymptotically stable. It must be cautioned that, however, the system may go unstable if the stability of the PID controller (26a) is violated due to the coupling with the virtual object dynamics (6) and the environment response $f = K_e p$.

V. EXPERIMENTS

A. Setup

The proposed controller (36) was experimentally tested by using the 6-DOF industrial robot MOTOMAN-HP3J (Yaskawa Electric Corporation) shown in Fig. 3. The robot was controlled with a PC running the ART-Linux operating system, and had six AC servomotors, which were integrated with harmonic-drive gearings and optical encoders. A six-axis force sensor (Nitta Corporation) was attached on the tip of the robot, and a bolt with a circular head was installed on the force sensor, as can be seen in Fig. 3(a).

As shown in Fig. 3(a), an aluminum pole was fixed to the base of the robot. In order to test the contact with an almost rigid environment and a compliant environment, the end-effector (i.e., the bolt head) was controlled to make contact directly with the aluminum pole (Fig. 3(b)) or with a sheet of sponge rubber attached to the pole (Fig. 3(c)). In most experiments (except Experiment IV), only the base joint was used, and the other joints were controlled to maintain a constant angle so that the end-effector should make contact with the "environment" (the aluminum pole or the rubber sheet) when the base joint rotated. In the following descriptions, all



(a) Motoman HP3J and aluminum pole



(b) contact with aluminum pole



(c) contact with rubber sheet

Fig. 3. Experimental setup

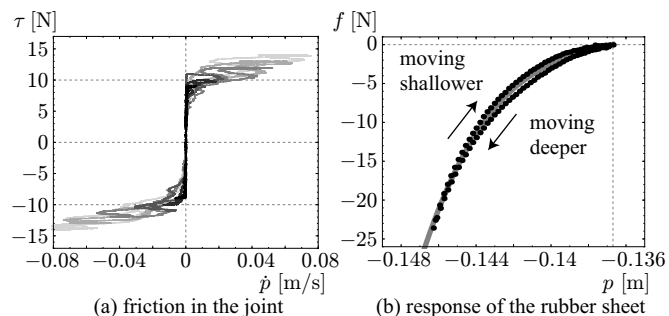


Fig. 4. Properties of the experimental setup. (a) \dot{p} - τ curves obtained from the sinusoidal input of τ with the frequency 0.17 Hz and different magnitudes, without contact at the end-effector. Different colors indicate results obtained with different magnitudes of τ . (b) The p - f curve produced by the contact between the end-effector and the rubber sheet. The black points indicate data measured every 1 s during a pushing motion and the gray curve represents the fitting curve $f = -\phi(-p - 0.137)$ where $\phi(x) \triangleq 7.02 \times 10^7 x^{3.28} + 600x$.

quantities were measured in the translational system along the circular arc path (with the radius of 0.44 m) of the end-effector, which is correspondent to the rotational system around the first joint.

The gear ratio of the base joint was 100. Through preliminary experiments, it was found that the magnitude of friction torque in the base joint was about 4.4 N-m, which was equivalent to 10 N at the end-effector position, as shown in Fig. 4(a). The relation between the end-effector's position and the contact force from the rubber sheet was obtained as shown in Fig. 4(b), which shows that the spring coefficient of the rubber sheet at shallow indentation was about 600 N/m.

In the experiments, the base joint was controlled by an admittance controller with the time-step size $T = 0.001$ s. The

virtual object dynamics (6) was implemented as the following discrete-time controller:

$$v_d(k) := (bv_d(k-1) - T(f(k) - f_d(k))) / (mT + b) \quad (40a)$$

$$p_d(k) := p_d(k-1) + Tv_d(k). \quad (40b)$$

The parameters for (40) were chosen as $m = 5$ kg and $b = 5$ N·s/m when the aluminum pole was used, and as $m = 1$ kg and $b = 1$ N·s/m when the rubber sheet was used. These values were chosen as low as the system remained stable. Choosing different values for different contact materials can be justified by considering that it is practically reasonable to set the values as small as possible according to the maximum possible stiffness of the environment for individual application scenarios. Note that the proposed controller is not for guaranteeing the system stability in contact with arbitrarily stiff environments.

As the internal position controller of the admittance controller, the following six control schemes were used.

- **PSMC2+AFF**: Proposed control law (36).
- **PSMC2**: (36) with $M = 0$.
- **PSMC+AFF**: (36) with $J = 0$.
- **PSMC**: (36) with $M = 0$ and $J = 0$, i.e., Equation (32) of [11].
- **SPID+AFF**: Saturated PID control law with acceleration feedforward, i.e., (7) with $|\tau|$ being bounded by F .
- **SPID**: Saturated PID control law, i.e., (7) with $M = 0$ and $|\tau|$ being bounded by F .

Unless otherwise specified, the parameters for the internal position controllers were chosen as; $K = 60000$ N/m, $B = 1000$ N·s/m, $L = 90000$ N/m/s, $F = 20$ N, $H = 0.4$ s, $J = 0.04$ s², $M = 10$ kg. The gains K , B , and L were chosen as high as the system remained stable, and F was set adequately larger than the magnitude of the friction force in the joint. The H and J values were chosen to result in the critical damping of the time constant of 0.2 s considering previously reported implementations [44], [45] of PSMC.

The value of M was chosen so that it realizes stable contact with the controller PSMC2+AFF. Smaller M values resulted in instability or oscillation (as seen in the upcoming results) and larger M values resulted in high-frequency vibration in τ due to the magnified noise in f from the force sensor. From a theoretical point of view, M should be chosen considering the inertia of the controlled system (M_r in Section III). In the setup, however, M_r was difficult to estimate because the controlled system was not a single mass, but was composed of at least two masses (the link and the motor) connected by the harmonic drive gearing, which is elastic. It might be possible to enhance the stability by replacing τ_f in (36) by a more sophisticated feedforward term considering the two-mass structure of the controlled system, such as the one employed in [30], but it falls outside scope of this paper.

Internal position controllers other than the listed six controllers were not considered because post-saturation behaviors of position controllers have been already discussed elsewhere [11], including empirical comparison between PSMC and anti-windup PID control [46]. Force control schemes without internal position loops were not compared either because

the performance of those controllers strongly depends on the dynamics of the robot including the joint friction.

B. Experiment I: Pushing with Varying Force

In this set of experiments, the robot was controlled to maintain contact with the environment with a specified desired force. The robot was initially set in a light contact with the environment before the admittance controller was initiated. The desired force f_d was switched between -8 N and -3 N every 0.5 s.

Fig. 5 shows the results obtained with the two types of environments and the six internal position controllers. Here, $f \geq 0$ means that the robot was not in contact with the environment at that time. It is clearly seen that the inclusion of AFF ($M > 0$) resulted in smaller bouncing and oscillation and better tracking of the contact force. The advantage of PSMC2 over PSMC and SPID (all with AFF) is observed only after the saturation in τ . It is as expected because PSMC2 and PSMC are equivalent to SPID when the actuator is not saturated. In the case of the aluminum pole and the heavier virtual object, the actuator saturation was less frequent due to the small movement of the virtual object.

Fig. 6 shows the results of PSMC2+AFF and PSMC+AFF in Fig. 5(b) in different colors and time scales. The difference between PSMC+AFF ($J = 0$) and PSMC2+AFF ($J > 0$) can be seen at transitions from the reaching mode ($|\tau| = F$) to the sliding mode ($|\tau| < F$), which are highlighted by the gray circles. It is shown that the changes in the actuator force τ are abrupt with PSMC+AFF ($J = 0$) while they are rather continuous with PSMC2+AFF ($J > 0$).

C. Experiment II: Pushing after Collision

In the second set of experiments, the robot was initially set about 0.01 m away from the environment, and the desired force was fixed at $f_d = 5$ N. After the collisions, the robot showed stronger tendency of bouncing than it was in Experiment I in both cases of the two environments. The controller PSMC2+AFF with different values of J and M (including PSMC+AFF and PSMC2 as special cases) was used to show the effects of those parameters. Any J values larger than $H^2/4$ were not tried because it is theoretically clear that they result in underdamped (overshooting) converging trajectories of p toward p_d after a transition from the reaching (saturated) mode to the sliding (unsaturated) mode.

Fig. 7 shows the results. It can be seen that, in both cases of the aluminum pole and the rubber sheet, an increased M resulted in a reduced magnitude of oscillation. It is also shown that an increased J resulted in a reduced magnitude of bouncing, as well as a reduced oscillation. These results indicate the necessity of $M > 0$ and $J > 0$ in the new position controller.

D. Experiment III: Moving by Hand

In this experiment, the experimenter grasped the end-effector and moved it cyclically at the frequency of approximately 1 Hz, being paced by a metronome. This experiment

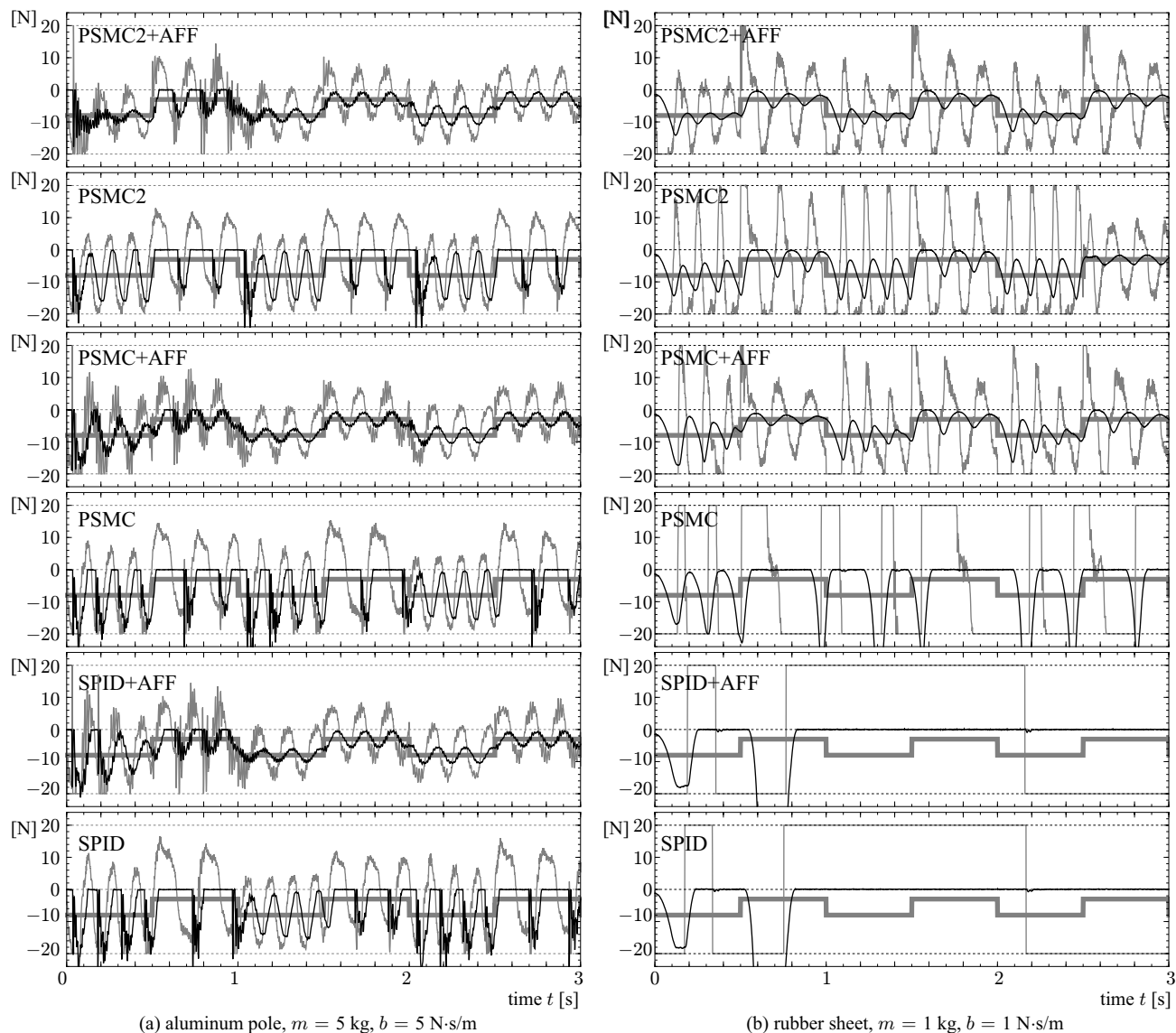


Fig. 5. Results of Experiment I: the measured force f (black thin), the actuator force τ (gray thin), and the desired force f_d (gray thick).

was performed considering the application to physical human-robot interaction [4]–[9]. The virtual object parameters were set as $m = 1$ kg and $b = 1$ N·s/m. For this experiment, only PSMC2+AFF, PSMC+AFF, and SPID+AFF were used because removing AFF did not cause any significant difference, presumably due to the constraint imposed by the experimenter's hand being soft enough. The desired force was set constant at $f_d = 0$ N.

Fig. 8 shows the data of the position p , the measured force f , and the actuator force τ obtained with the three internal position controllers. It should be noted that the actuator force τ was saturated almost all the time with all controllers because the force limit ($F = 20$ N) was not high enough to track the virtual object's motion induced by the experimenter's force. Fig. 8(c) shows that SPID+AFF resulted in distinctly poor performance, which did not allow the intended cyclic movement. Meanwhile, Fig. 8(a) and (b) show that the inclusion of $J > 0$

in the controller resulted in smaller and smoother fluctuation in the contact force, which means that the experimenter was able to move the robot more smoothly and easily than he was with $J = 0$. The p - f plot in Fig. 8(b) shows that, when the experimenter changed the direction of his motion, the controller with $J = 0$ produced resisting force against the experimenter's motion and thus a large force was produced between the experimenter's hand and the end-effector. That is, one can infer that the $J > 0$ contributes quicker response even in the actuator force saturation and that it results in smooth motion of the robot and smooth change in the contact force.

E. Experiment IV: Moving by Hand with 6-DOF Control

A set of 6-DOF experiments was performed, in which the admittance controller was implemented to each of the six joints of the robot. The force inputs to the joint admittance controllers were obtained by multiplying the measured force

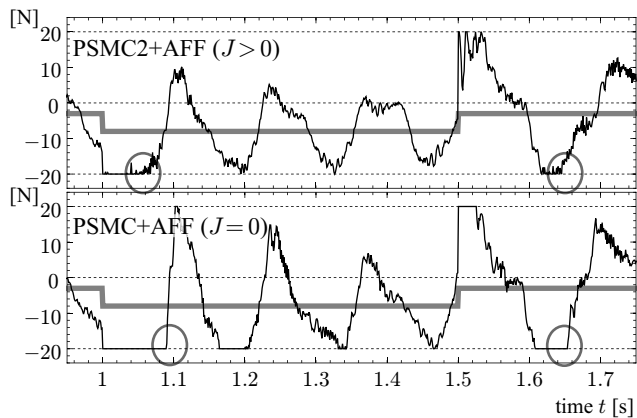


Fig. 6. Enlarged views of Fig. 5(b) in different colors: the actuator force τ (black) and the desired force f_d (gray thick). The gray circles highlight transitions from the reaching mode to the sliding mode, where the difference between the two controllers is distinct.

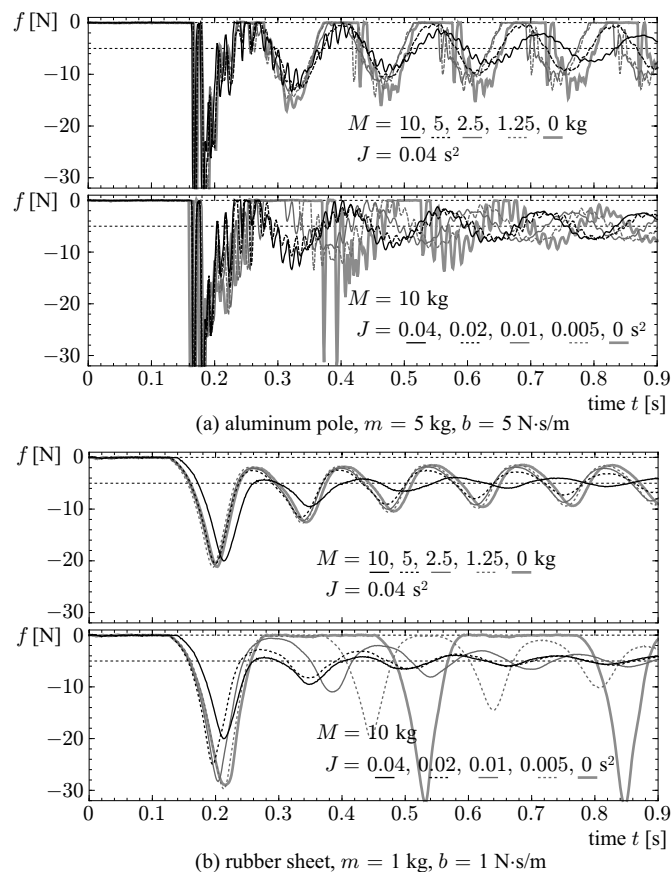


Fig. 7. Results of Experiment II: the measured force f with different values of M (top) and J (bottom) for each of the two environments. Different line styles indicate different values of M or J , as indicated by the lines under the numerics in the graphs.

at the end-effector by the transpose Jacobian. The desired force f_d was set zero in every joint. The experimenter grasped the end-effector and intended to move it along circular trajectories.

The parameters for the joint controllers were chosen as in Table I. As high values for K , B , L and M and as low values for m and b were chosen as the system did not exhibit vibratory or unstable behaviors. The torque limits F

TABLE I
PARAMETER VALUES USED IN EXPERIMENT IV

joint #		1	2	3	4	5	6
K	N·m/rad	30000	100000	21000	6000	6000	3000
B	N·m·s/rad	200	600	140	40	40	20
L	N·m/rad/s	10000	30000	7000	2000	2000	1000
M	kg·m ²	8	8	8	1	1	1
F	N·m	15	25	7	20	20	20
m	kg·m ²	0.3	0.3	0.3	0.5	0.5	0.5
b	N·m·s/rad	0.3	0.3	0.3	0.5	0.5	0.5

were determined so that the torques easily saturate in the task performed in this experiment. The values of H and J were set as $H = 0.2$ s and $J = 0.04$ s² for every joint. For comparison, the three internal position controllers (PSMC2+AFF, PSMC+AFF, and SPID+AFF) were used.

In the use of six joints, the system was more prone to instability than in the use of a single joint, likely due to the compliance of the joints. Preliminary experiments showed that increasing M values slightly improved the stability but intensified high-frequency vibration. It can be attributed to the noise in the measured force magnified through the feedforward term τ_f . Thus, the noise reduction filter proposed in [47], which has been shown to produce relatively small phase lag [48], was applied to all six components of the measured force.

Fig. 9 shows the result. With SPID+AFF, the experimenter was unable to draw a circular trajectory due to the resistive force from the robot. With PSMC2+AFF and PSMC+AFF, he was able to draw circles, but it can be seen that smoother movement was achieved with PSMC2+AFF. The nonsmooth behaviors of PSMC+AFF are also visible as the peaks in the graph of $\|f\|$. These results indicate the effectiveness of PSMC2+AFF also in the multidimensional case.

VI. CONCLUSIONS

This paper has presented a position controller that is suited for the use as the internal position controller of an admittance controller. The proposed controller is an extension of PSMC [11], and is advantageous especially in applications where the robot is required to continue operation even when the actuator force is saturated. The new controller was motivated by preliminary analysis on a sliding mode position controller that involves acceleration feedback, although the direct acceleration feedback is avoided in the new controller. The new controller realizes smooth transitions between saturated periods and unsaturated periods, and it quickly responds to changes in the applied force even in saturated periods. The controller was tested through experiments employing a robot with harmonic drive gearing and a force sensor, showing better force control and smooth motion.

The paper has only considered the application of the proposed position controller as the internal position controller of an admittance controller. The proposed controller, however, is essentially independent from admittance control. Thus, the proposed controller could be used in other applications if its properties are beneficial to those applications. Force-reflecting teleoperators [49], [50], of which the slave robot is position-controlled, might be another example of potential applications.

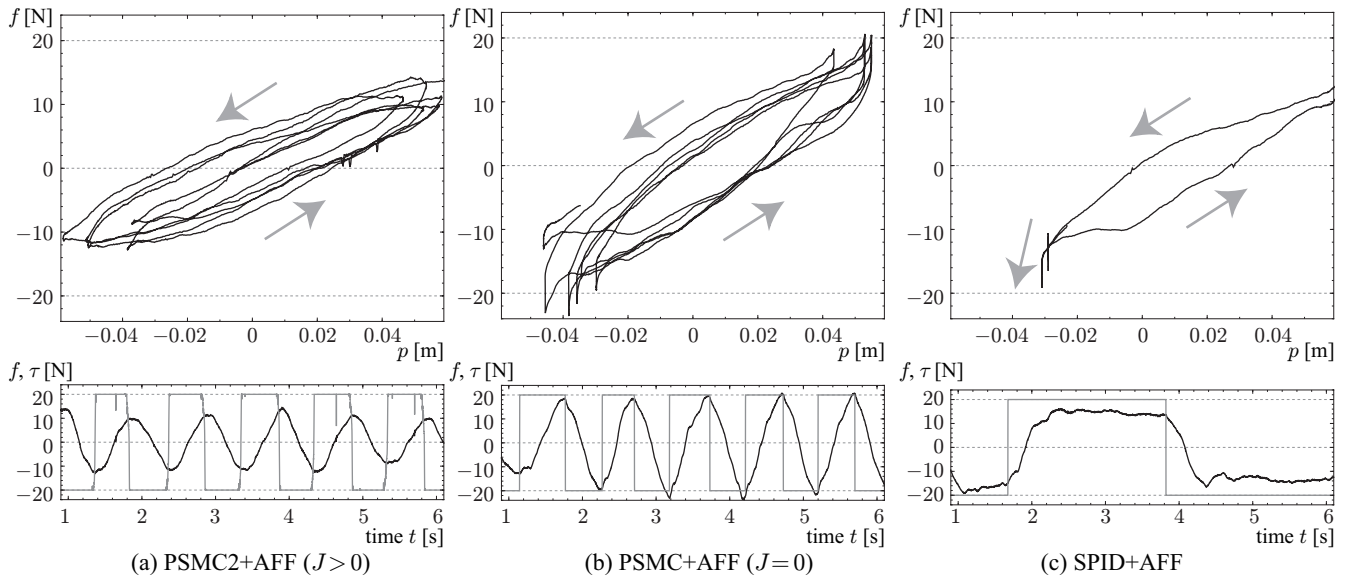


Fig. 8. Results of Experiment III: the end-effector was moved by the experimenter's hand at the frequency of approximately 1 Hz. The upper graphs show the relation between the end-effector position p and the measured force f . The lower graphs show the measured force f (black) and the actuator force τ (gray).

This paper has validated the proposed controller mostly empirically. Its theoretical properties has been discussed in sections III-D and IV-C based on an approximated controller with $K \rightarrow \infty$. A more strict analysis on the controller, which is described as the differential-algebraic equation (26), is remained as an open problem. One potential difficulty in such analysis lies in the fact that (26) includes \ddot{u} only in the argument of sgn function, which prevents its conversion into the standard form of state-space representation. Stability analysis on practical scenarios of admittance control, such as the case of unilateral constraint (e.g., $f = \min(0, K_e p)$), should also be addressed in future study.

To further enhance the stability in the unsaturated period, the feedforward term $\tau_f = M\ddot{p}_d$ in the proposed controller could be improved. For example, this term could be replaced by a more complicated term, such as those involving centrifugal and Coriolis forces, joint friction, and joint compliance [30]. It would also be possible to apply phase lead to the force signal with appropriate noise filtering, as has been empirically demonstrated in [48]. These approaches may be effective to attenuate the instability caused by the non-collocation [23], [27] between the force sensor and the actuators.

Multi-DOF implementation of the proposed method was tested in section V-E through joint-space admittance control. It is, however, still unclear how the saturation at each joint influences task-space behavior of the end-effector. Another possible way would be to define the virtual object dynamics in the task space and to perform the position control in a transpose Jacobian-based method. It, however, will need a non-trivial extension of the proposed controller to deal with position and attitude in the three-dimensional Cartesian space. It would also be useful to extend the proposed method to allow inverse kinematics-based implementation with appropriate singularity management, such as those presented in [51].

Acknowledgment

This work was supported by Grant-in-Aid for Scientific Research (B), No. 22760321, from Japan Society for the Promotion of Science.

APPENDIX

This appendix provides proofs of Propositions 1 and 2, which represent the asymptotic stability of controllers employing PDD²-type sliding mode control (15).

Proof of Proposition 1: Considering the fact that substituting (15) into (5) yields (19), one can describe the system dynamics as follows:

$$\ddot{p} = (F/M_r)\text{sat}(M_r(p_d - p - H\dot{p})/(FJ)). \quad (41)$$

Let us define the following Lyapunov function candidate:

$$V(p, \dot{p}) \triangleq \frac{M_r \dot{p}^2}{2} + \frac{F^2 J}{M_r} \text{Isat} \left(\frac{M_r(p_d - p - H\dot{p})}{FJ} \right) \quad (42)$$

where

$$\text{Isat}(x) \triangleq \begin{cases} x^2/2 & \text{if } |x| < 1 \\ \text{sgn}(x)x - 1/2 & \text{otherwise.} \end{cases} \quad (43)$$

Then, its time derivative is obtained as follows:

$$\dot{V}(p, \dot{p}) = -\frac{HF^2}{M_r} \left(\text{sat} \left(\frac{M_r(p_d - p - H\dot{p})}{FJ} \right) \right)^2 \leq 0. \quad (44)$$

In the light of LaSalle's Invariance theorem, one can easily see that the system is globally asymptotically stable. ■

Proof of Proposition 2: Considering the fact that substituting (15) into (5) yields (19), one can describe the system dynamics as follows:

$$\ddot{p}_d = (f_d - K_e p - b\dot{p}_d)/m \quad (45)$$

$$\ddot{p} = (F\text{sat}(\beta + f_d/F) - K_e p)/M_r \quad (46)$$

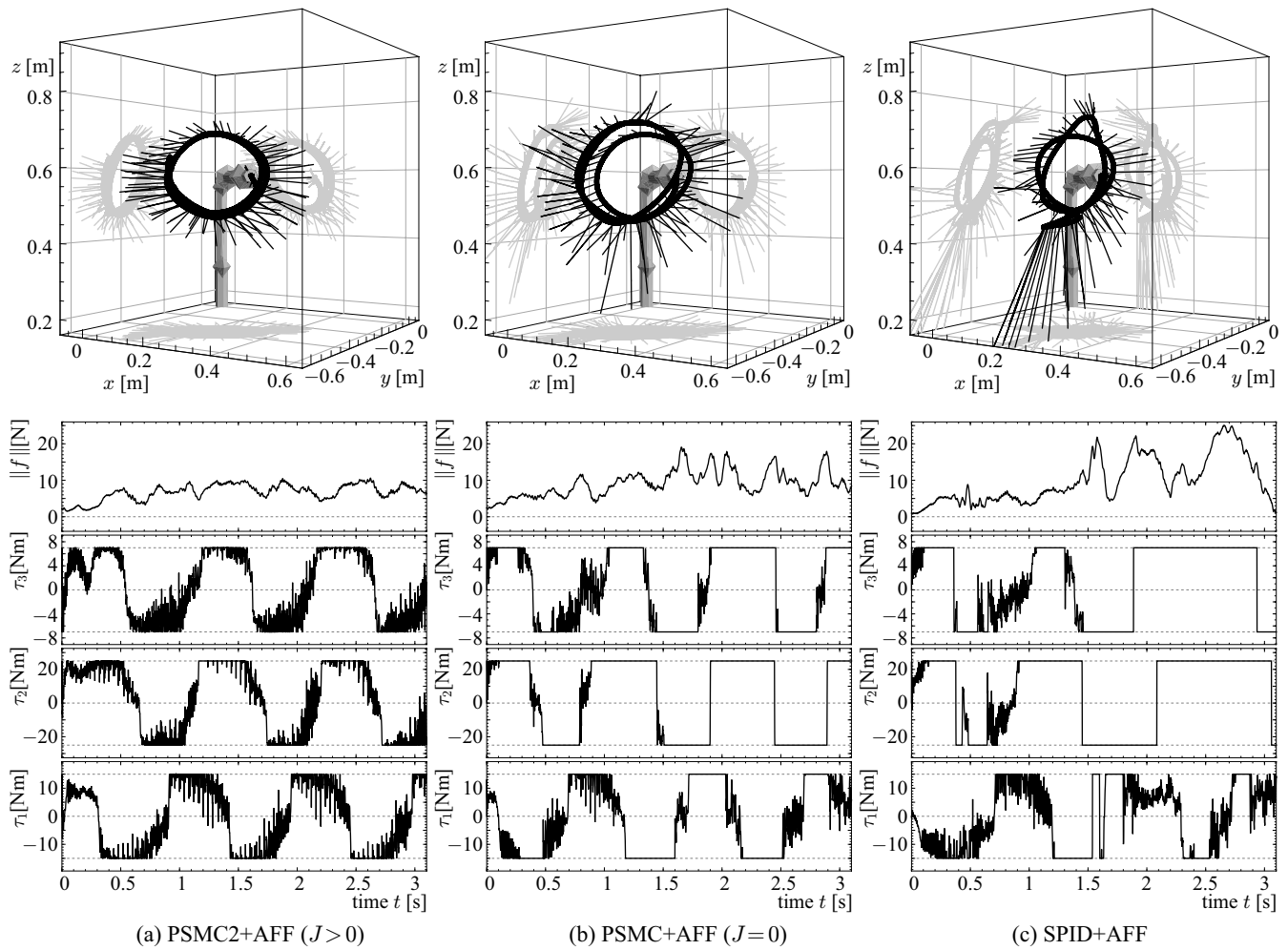


Fig. 9. Results of Experiment IV: the end-effector was moved by the experimenter's hand to draw a circular trajectory. The upper graphs show the trajectories of p (black thick), the force vectors $-f$ (black thin, scaled by a factor of 0.015 m/N), and the initial configuration of the robot. Projections of the trajectories and the forces are drawn in gray. The lower graphs show $\|f\|$ and τ of the joints 1 to 3 from the base, at which actuator saturation primarily occurred.

where

$$\beta \triangleq \frac{M_r}{F} \left(\frac{f_d - K_e p - b \dot{p}_d}{m} + \frac{s}{J} \right) + \frac{K_e p - f_d}{F}. \quad (47)$$

Based on this, the state-space representation of the system can be described in the following form:

$$\dot{\mathbf{x}} = \mathbf{A}\mathbf{x} + \mathbf{b} \text{dzn}(\beta + f_d/F) \quad (48)$$

where

$$\text{dzn}(x) \triangleq x - \text{sat}(x) \quad (49)$$

$$\mathbf{x} \triangleq [\beta \quad p - f_d/K_e \quad \dot{p} \quad \dot{p}_d]^T \quad (50)$$

and $\mathbf{A} \in \mathbb{R}^{4 \times 4}$ and $\mathbf{b} \in \mathbb{R}^4$ are appropriate constant matrices.

By examining the entries of the matrix \mathbf{A} , one can easily see that \mathbf{A} is Hurwitz. Therefore, there exists a pair of 4×4 symmetric positive definite matrices \mathbf{P} and \mathbf{Q} that satisfies $\mathbf{P}\mathbf{A} + \mathbf{A}^T\mathbf{P} = -\mathbf{Q}$. By using such a \mathbf{P} , let us define the following Lyapunov function candidate:

$$V(\mathbf{x}) \triangleq \mathbf{x}^T \mathbf{P} \mathbf{x} + \text{Idzn}(\beta + f_d/F) \quad (51)$$

where

$$\text{Idzn}(x) \triangleq (x - \text{sat}(x))^2/2, \quad (52)$$

which satisfies $V(\mathbf{x}) > 0$ for all $\mathbf{x} \neq \mathbf{0}$ if $|f_d| < F$. Its time derivative is obtained as follows:

$$\begin{aligned} \dot{V}(\mathbf{x}) = & -\mathbf{x}^T \mathbf{Q} \mathbf{x} - (H/J) \text{dzn}(\beta + f_d/F) \times \\ & (\text{sat}(\beta + f_d/F) - J\xi(\mathbf{x})/H - f_d/F) \end{aligned} \quad (53)$$

where

$$\xi(\mathbf{x}) \triangleq a_{12}(p - f_d/K_e) + a_{13}\dot{p} + a_{14}\dot{p}_d + 2\mathbf{x}^T \mathbf{P} \mathbf{b}. \quad (54)$$

Equation (53) means that $\dot{V}(\mathbf{x}) < 0$ for all $\mathbf{x} \in \mathcal{D} \setminus \mathbf{0}$ where

$$\mathcal{D} \triangleq \{\mathbf{x}; |\beta + f_d/F| < 1 \vee |J\xi(\mathbf{x})/H + f_d/F| < 1\}, \quad (55)$$

which includes the origin if $|f_d| < F$. This means that, under the condition that $|f_d| < F$, the system is (locally) asymptotically stable. ■

REFERENCES

- [1] D. E. Whitney, "Historical perspective and state of the art in robot force control," *Int. J. Robotics Research*, vol. 6, no. 1, pp. 3–14, 1987.
- [2] G. Zeng and A. Hemami, "An overview of robot force control," *Robotica*, vol. 15, pp. 473–482, 1997.
- [3] C. Ott, R. Mukherjee, and Y. Nakamura, "Unified impedance and admittance control," in *Proc. IEEE Int. Conf. Robotics and Automation*, 2010, pp. 554–561.

- [4] M. Ueberle and M. Buss, "Control of kinesthetic haptic interfaces," in *Proc. Workshop on Touch and Haptics, IEEE/RSJ Int. Conf. Intelligent Robots and Systems*, 2004, pp. 1–14.
- [5] R. Q. Van Der Linde and P. Lammertse, "HapticMaster – a generic force controlled robot for human interaction," *Industrial Robot*, vol. 30, no. 6, pp. 515–524, 2003.
- [6] A. Peer and M. Buss, "A new admittance-type haptic interface for bimanual manipulations," *IEEE/ASME Trans. Mechatronics*, vol. 13, no. 4, pp. 416–428, 2008.
- [7] P. R. Culmer, A. E. Jackson, S. Makower, R. Richardson, J. A. Cozens, M. C. Levesley, and B. B. Bhakta, "A control strategy for upper limb robotic rehabilitation with a dual robot system," *IEEE/ASME Trans. Mechatronics*, vol. 15, no. 4, pp. 575–585, 2010.
- [8] J. A. Saglia, N. G. Tсарarakis, J. S. Dai, and D. G. Caldwell, "Control strategies for patient-assisted training using the ankle rehabilitation robot (ARBOT)," *IEEE/ASME Trans. Mechatronics*, vol. 18, no. 6, 2013, 10.1109/TMECH.2012.2214228.
- [9] N. Takesue, H. Murayama, K. Fujiwara, K. Matsumoto, H. Konosu, and H. Fujimoto, "Kinesthetic assistance for improving task performance — the case of window installation assist —," *Int. J. Automation Technology*, vol. 3, no. 6, pp. 663–670, 2009.
- [10] H. Arai, "Force-controlled metal spinning machine using linear motors," in *Proc. IEEE Int. Conf. Robotics and Automation*, 2006, pp. 4031–4036.
- [11] R. Kikuuwe, S. Yasukouchi, H. Fujimoto, and M. Yamamoto, "Proxy-based sliding mode control: A safer extension of PID position control," *IEEE Trans. Robotics*, vol. 26, no. 4, pp. 860–873, 2010.
- [12] J. De Schutter, "A study of active compliant motion control methods for rigid manipulators based on a generic scheme," in *Proc. IEEE Int. Conf. Robotics and Automation*, vol. 4, 1987, pp. 1060–1065.
- [13] H. Ishikawa, C. Sawada, K. Kawase, and M. Takata, "Stable compliance control and its implementation for a 6 DOF manipulator," in *Proc. IEEE Int. Conf. Robotics and Automation*, vol. 1, 1989, pp. 98–103.
- [14] H. Seraji, "Adaptive admittance control: an approach to explicit force control in compliant motion," in *Proc. IEEE Int. Conf. Robotics and Automation*, 1994, pp. 2705–2712.
- [15] D. E. Whitney, "Force feedback control of manipulator fine motions," *Trans. ASME: J. Dynamic Systems, Measurement, and Control*, vol. 99, no. 2, pp. 91–97, 1977.
- [16] G. Hirzinger, "Direct digital robot control using a force-torque sensor," in *Proc. IFAC Symp. Real Time Digital Control Applications*, 1983, pp. 243–255.
- [17] J. De Schutter and H. Van Brussel, "A methodology for specifying and controlling compliant robot motion," in *Proc. Conf. Decision and Control*, 1986, pp. 1871–1876.
- [18] J. A. Maples and J. J. Becker, "Experiments in force control of robotic manipulators," in *Proc. IEEE Int. Conf. Robotics and Automation*, 1986, pp. 695–702.
- [19] K. Kosuge, K. Furuta, and T. Yokoyama, "Virtual internal model following control of robot arms," in *Proc. IEEE Int. Conf. Robotics and Automation*, 1987, pp. 1549–1554.
- [20] D. A. Lawrence and R. M. Stoughton, "Position-based impedance control – achieving stability in practice," in *Proc. AIAA Guidance, Navigation and Control Conference*, 1987, pp. 221–226.
- [21] D. Šurdilović and J. Kirchhof, "A new position based force/impedance control for industrial robots," in *Proc. IEEE Int. Conf. Robotics and Automation*, 1996, pp. 629–634.
- [22] D. A. Lawrence, "Impedance control stability properties in common implementation," in *Proc. IEEE Int. Conf. Robotics and Automation*, 1988, pp. 1185–1190.
- [23] S. D. Eppinger and W. P. Seering, "Understanding bandwidth limitations in robot force control," *Proc. IEEE Int. Conf. Robotics and Automation*, vol. 4, pp. 904–909, 1987.
- [24] T. Valency and M. Zacksenhouse, "Accuracy/robustness dilemma in impedance control," *Trans. ASME: J. Dynamic Systems, Measurement, and Control*, vol. 125, no. 3, pp. 310–319, 2003.
- [25] S. H. Kang, M. Jin, and P. H. Chang, "A solution to the accuracy/robustness dilemma in impedance control," *IEEE/ASME Trans. Mechatronics*, vol. 14, no. 3, pp. 282–294, 2009.
- [26] W. S. Newman, "Stability and performance limits of interaction controllers," *Trans. ASME: J. Dynamic Systems, Measurement, and Control*, vol. 114, no. 4, pp. 563–570, 1992.
- [27] M. Dohring and W. S. Newman, "The passivity of natural admittance control implementations," in *Proc. IEEE Int. Conf. Robotics and Automation*, 2003, pp. 3710–3715.
- [28] J. J. González and G. R. Widmann, "A force commanded impedance control scheme for robots with hard nonlinearities," *IEEE Trans. Control Systems Technology*, vol. 3, no. 4, pp. 398–408, 1995.
- [29] S. Tafazoli, S. E. Salcudean, K. Hashtrudi-Zaad, and P. D. Lawrence, "Impedance control of a teleoperated excavator," *IEEE Trans. Control Systems Technology*, vol. 10, no. 3, pp. 355–367, 2002.
- [30] G. Ferretti, G. Magnani, and P. Rocco, "Impedance control for elastic joints industrial manipulators," *IEEE Trans. Robotics and Automation*, vol. 20, no. 3, pp. 488–498, 2004.
- [31] J. J. González and G. R. Widmann, "Investigation of nonlinearities in the force control of real robots," *IEEE Trans. Systems, Man, and Cybernetics*, vol. 22, no. 5, pp. 1183–1193, 1992.
- [32] R. Volpe and P. K. Khosla, "A theoretical and experimental investigation of explicit force control strategies for manipulators," *IEEE Trans. Automatic Control*, vol. 38, no. 11, pp. 1634–1650, 1993.
- [33] L. S. Wilfinger, J. T. Wen, and R. R. Murphy, "Integral force control with robustness enhancement," *IEEE Control Systems*, vol. 14, no. 1, pp. 31–40, 1994.
- [34] C. C. Cheah, S. P. Hou, Y. Zhao, and J.-J. E. Slotine, "Adaptive vision and force tracking control for robots with constraint uncertainty," *IEEE/ASME Trans. Mechatronics*, vol. 15, no. 3, pp. 389–399, 2010.
- [35] W. S. Newman and Y. Zhang, "Stable interaction control and Coulomb friction compensation using natural admittance control," *J. Robotic Systems*, vol. 11, no. 1, pp. 3–11, 1994.
- [36] A. Šabanović, M. Elitaš, and K. Ohnishi, "Sliding modes in constrained systems control," *IEEE Trans. Industrial Electronics*, vol. 55, no. 9, pp. 3332–3339, 2008.
- [37] S. Katsura and K. Ohnishi, "Modal system design of multirobot systems by interaction mode control," *IEEE Trans. Industrial Electronics*, vol. 54, no. 3, pp. 1537–1546, 2007.
- [38] K. Ohnishi, M. Shibata, and T. Murakami, "Motion control for advanced mechatronics," *IEEE/ASME Trans. Mechatronics*, vol. 1, no. 1, pp. 56–67, 1996.
- [39] S. Chiaverini, B. Siciliano, and L. Villani, "A survey of robot interaction control schemes with experimental comparison," *IEEE/ASME Trans. Mechatronics*, vol. 4, no. 3, pp. 273–285, 1999.
- [40] G. V. Smirnov, *Introduction to the Theory of Differential Inclusions*. Providence, RI, USA: American Mathematical Society, 2002.
- [41] J.-J. E. Slotine, "The robust control of robot manipulators," *Int. J. Robotics Research*, vol. 4, no. 2, pp. 49–63, 1985.
- [42] V. I. Utkin, J. Guldner, and J. Shi, *Sliding Mode Control in Electro-Mechanical Systems*, 2nd ed. Boca Raton, FL, USA: CRC Press, 2009.
- [43] D. C. Ruspini, K. Kolarov, and O. Khatib, "The haptic display of complex graphical environments," in *Proc. ACM SIGGRAPH 97*, 1997, pp. 345–352.
- [44] R. Kikuuwe, T. Yamamoto, and H. Fujimoto, "A guideline for low-force robotic guidance for enhancing human performance of positioning and trajectory tracking: It should be stiff and appropriately slow," *IEEE Trans. Systems, Man and Cybernetics, Part A: Systems and Humans*, vol. 38, no. 4, pp. 945–957, 2008.
- [45] M. Van Damme, B. Vanderborght, B. Verrelst, R. Van Ham, F. Daerden, and D. Lefeber, "Proxy-based sliding mode control of a planar pneumatic manipulator," *Int. J. Robotics Research*, vol. 28, no. 2, pp. 266–284, 2009.
- [46] Y. Li, K. H. Ang, and G. C. Y. Chong, "PID control system analysis and design," *IEEE Control Syst. Mag.*, vol. 26, no. 1, pp. 32–41, 2006.
- [47] S. Jin, R. Kikuuwe, and M. Yamamoto, "Real-time quadratic sliding mode filter for removing noise," *Advanced Robotics*, vol. 26, no. 8-9, pp. 877–896, 2012.
- [48] S. Jin, R. Kikuuwe, and M. Yamamoto, "Parameter selection guidelines for a parabolic sliding mode filter based on frequency and time domain characteristics," *J. Control Science and Engineering*, vol. 2012, article 923679, 2012.
- [49] H. I. Son, T. Bhattacharjee, and H. Hashimoto, "Enhancement in operator's perception of soft tissues and its experimental validation for scaled teleoperation systems," *IEEE/ASME Trans. Mechatronics*, vol. 16, no. 6, pp. 1096–1109, 2011.
- [50] Z. T. H. Tse, H. Elhawary, M. Rea, B. Davies, I. Young, and M. Lamperth, "Haptic needle unit for MR-guided biopsy and its control," *IEEE/ASME Trans. Mechatronics*, vol. 17, no. 1, pp. 183–187, 2012.
- [51] R. V. Patel, H. A. Talebi, J. Jayender, and F. Shadpey, "A robust position and force control strategy for 7-DOF redundant manipulators," *IEEE/ASME Trans. Mechatronics*, vol. 14, no. 5, pp. 575–589, 2009.



Ryo Kikuwe (S'02-M'03) received the B.S., M.S., and Ph.D.(Eng.) degrees from Kyoto University, Kyoto, Japan, in 1998, 2000, and 2003, respectively, all in mechanical engineering.

From 2003 to 2007, he was an Endowed-Chair Research Associate at Nagoya Institute of Technology, Nagoya, Japan. He is currently an Associate Professor at the Department of Mechanical Engineering, Kyushu University, Fukuoka, Japan. His research interests include physical human-robot interaction, realtime simulation for haptic rendering

and physics-based animation, and engineering applications of differential inclusions.

Prof. Kikuwe is a member of the Robotics Society of Japan, the Japan Society of Mechanical Engineers, the Society of Instrument and Control Engineers (Japan), and the Virtual Reality Society of Japan.